Mineralium Deposita (2004) 39: 265–281
DOI 10.1007/s00126-003-0396-6

ARTICLE

**Jean Vallance · Marie-Christine Boiron
Michel Cathelineau · Serge Fourcade · Michel Varlet
Christian Marignac**

The granite hosted gold deposit of Moulin de Chéni (Saint-Yrieix district, Massif Central, France): petrographic, structural, fluid inclusion and oxygen isotope constraints

Received: 21 June 2002 / Accepted: 23 October 2003 / Published online: 20 March 2004

Abstract The Moulin de Chéni orogenic gold deposit is the only granite-hosted deposit of the Saint-Yrieix district, French Massif Central. It occurs in 338 ± 1.5 Ma-old peraluminous leucogranites and is characterized by intense microfracturing and bleaching of the granite in relation to pervasive sulfide crystallization. Formation of quartz veins and gold deposition occurred in two successive stages: an early "mesozonal" stage of quartz-sulfide (Fe-As-S) deposition, usually devoid of gold and a late "epizonal" stage of base metal and gold deposition. Both stages postdate peak metamorphism and granite intrusion. The genesis of the deposit is the result of four successive fluid events: (1) Percolation of aqueous-carbonic metamorphic fluids under an assumed lithostatic regime of 400–450 °C, at a maximum depth of 13 km; (2) Formation of the main quartz lodes with coeval K-alteration and introduction of As and S from aqueous-carbonic fluids percolating along regional faults. Arsenopyrite and pyrite deposition was linked to the alteration of Fe-silicates into K-feldspar and phengite at near-constant iron content in the bulk granite. Temperature was similar to that of the preceding stage, but pressure decreased to 100–50 MPa, suggesting rapid uplift of the basement up to 7.5 km depth; (3) The resulting extensional tectonic leads to the deposition of gold, boulangerite, galena and sphalerite in brecciated arsenopyrite and pyrite from aqueous fluids during a mixing process. Temperature and salinity decrease from 280 to 140 °C and 8.1 wt% eq. NaCl to 1.6 wt% eq. NaCl, respectively; (4) Sealing of the late fault system by barren comb quartz which precipitated from dilute meteoric aqueous fluids (1.6 wt% eq. NaCl to 0.9 wt% eq. NaCl) under hydrostatic conditions at 200–150 °C.

Keywords Orogenic gold · Fluid mixing · Oxygen isotopes · P–T conditions · Variscan belt

Editorial handling: B. Lehmann

J. Vallance (✉) · M.-C. Boiron · M. Cathelineau
CREGU and UMR G2R 7566, BP 23,
54501 Vandoeuvre-lès-Nancy cedex, France
E-mail: jean.vallance@terre.unige.ch

J. Vallance
Section des Sciences de la Terre, Département de Minéralogie,
Rue des Maraîchers 13, 1205 Geneva, Switzerland

S. Fourcade
Géosciences Rennes, Campus de Beaulieu,
35042 Rennes cedex, France

M. Varlet
Société de Mines du Bourneix, Le Bourneix,
87500 Le Chalard, France

C. Marignac
CRPG-CNRS and Ecole des Mines, BP 20,
54501 Vandoeuvre-lès-Nancy cedex, France

Introduction

The French Massif Central is a major metalliferous province of the Variscan collision belt, hosting in particular U, W, Sb and Au deposits that formed from intense hydrothermal activity during the Neo-Variscan (late Carboniferous-early Permian, 330–290 Ma) period (Marignac and Cuney 1999).

The only gold deposits of the French Massif Central presently being mined are located in the western part, in the Saint-Yrieix district, comprising the Bourneix, Lauriéras and Moulin de Chéni mines (Figs. 1, 2). These mines have produced 8.7, 13 and 2.7 tons of gold, respectively, with a 10–15 g/t grade during the last two decades. Several deposits of the Saint-Yrieix district were the subject of detailed studies from structural (Bouchot et al. 1989; Nicaud 2001), mineralogical and geochemical (Touray et al. 1989; Chalier 1993; Esssarraj et al. 2001) points of view, allowing some generalizations about the characteristics of fluid circulation and ore deposition at the district scale (Boiron et al. 2000; Fourcade et al. 2000; Souhassou 2001). The main finding of these studies is the superposition of several deformation and fluid circulation events within the same

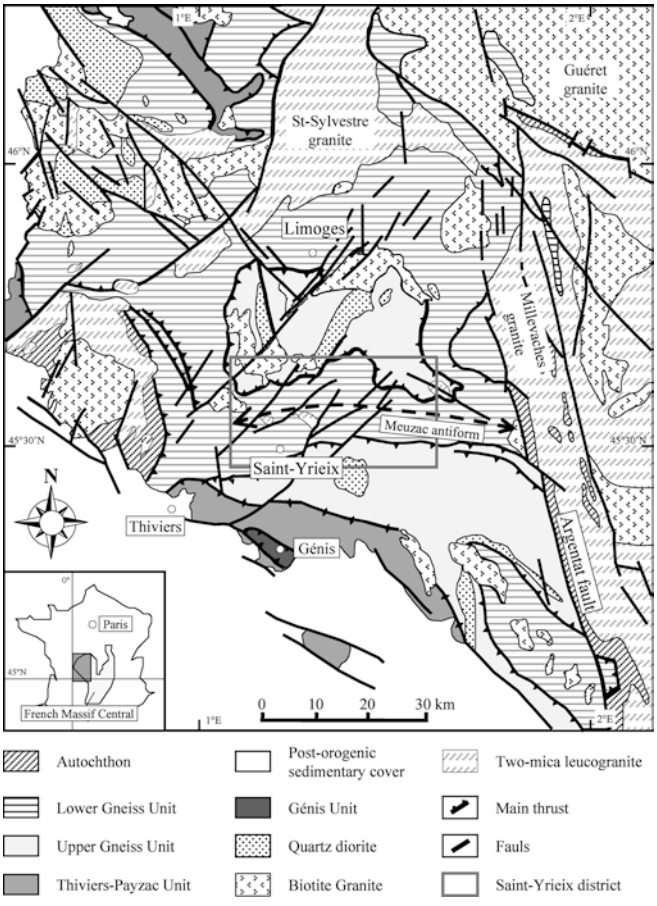

Fig. 1 Regional geological map showing the location of the Saint-Yrieix area with the main lithotectonic units of the northwestern French Massif Central (after Floc'h 1983)

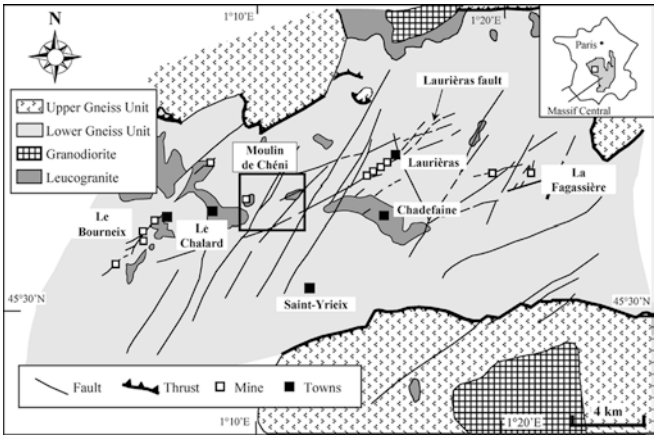

Fig. 2 Geological map of the Saint-Yrieix district showing the location of the main deposits and the studied area (modified from SMB-COGEMA, unpublished data). *Box* locates Fig. 3

channeling zones, e.g. in faults within metamorphic units, and that gold deposition occurred late in the history of fluid evolution. Nevertheless, our understanding remains hampered by the paucity of mineral markers in quartz-sealed faults that were affected by multiple deformation and recurrent mineral deposition, which could provide clues to the fluid evolution (Boiron et al. 1992). However, in granite-hosted deposits, deciphering the time/space relationships between deformation events, and the nature of the percolating fluids and mineralization stages is facilitated, since the microfissured granite is itself an excellent trap for the percolating fluids and may therefore contain a good record of the fluid/rock reactions. Moreover, granite-hosted gold deposits have recently received renewed attention, being possibly considered as representative of a new class of magmatic-hydrothermal gold deposits (Lang and Baker 2001).

The Moulin de Chéni deposit, in the Saint-Yrieix district, is the only granite-hosted gold deposit of the French Massif Central currently known, and is the target of the present study. The aim of this study was: (i) to decipher the succession of fluid circulation events by studying the relationships between microfractures in the granite, alteration events and ore deposition stages; and (ii) to reconstruct the P–T-t path of the mineralization/alteration process. The results are then compared with those of previous studies in the Saint-Yrieix district.

Geological setting

The western French Massif Central is comprised of several lithotectonic units that were stacked during the Meso-Variscan (Devonian-Early Carboniferous) period (Ledru et al. 1994a). Three main units are defined (Floc'h 1983; Ledru et al. 1994b) from top to bottom: the Upper Gneiss Unit, the Lower Gneiss Unit and the Autochthon (Fig. 1). The Upper Gneiss Unit contains paragneisses, leptynites and amphibolites of medium to high grade of Barrovian metamorphism, with numerous relics of eclogites and granulites (Santallier et al. 1988). The Upper Gneiss Unit is considered as a complex of terranes resulting from the Eo-Variscan (Cambrian-Silurian) stage of opening to closure of oceanic realms (Ledru et al. 1994b; Matte 1991). The Lower Gneiss Unit is made up of medium grade paragneisses, micaschists and orthogneisses, the latter derived from Cambrian to Ordovician granitoids, and is considered to have been initially part of the young Cadomian continental crust. The Autochthon has basically the same content as the Lower Gneiss Unit.

The French Massif Central is characterized during the Neo-Variscan stage by the interplay of compressional and extensional tectonics and voluminous granite magmatism. Compressional tectonics resulted in E–W folding of the Meso-Variscan pile and major transcurrent movements along crustal-scale shear zones (Arthaud and Matte 1977). In the Saint-Yrieix area (Fig. 1 and 2), the Meuzac antiform exposes the leptynites and micaschists of the Lower Gneiss Unit and a series of N060–080°E and N045–070°E trending ductile faults (Nicaud and Floc'h 2000) hosting the gold deposits. Post-collisional Stephanian-Permian NE–SW distension

was responsible for the Lauriéras fault and the reactivation of the previous N060–080°E and N045–070°E structures, as normal faults (Fig. 2) (Nicaud and Floc'h 2000). Several episodes of granite emplacement are recorded in the French Massif Central during the Neo-Variscan period (Marignac and Cuney 1999). In the Saint-Yrieix area this magmatism is of limited importance at the present erosion level, and consists of several granite stocks of km-size which intruded the Lower Gneiss Unit (Fig. 2): the Le Bourneix, Le Chalard and Chadefaine bodies (Stussi and La Roche 1984; Pastier 1992; Chalier 1993). These granites and their crosscutting aplo-pegmatite dykes are dated at 338.5 ± 1.5 Ma by the $^{39}Ar/^{40}Ar$ method (Alexandrov 2000). 30 km NE of Saint-Yrieix, the small leucogranite stock of La Porcherie was dated (U/Pb) at 317 ± 3 Ma by Lafon and Respaut (1988). Mafic magmatism (lamprophyre dykes) is widespread in the French Massif Central and is possibly related to the "basin and range" extensional tectonics during the Stephanian-Permian. In the Saint-Yrieix area, lamprophyre dykes occur at Lauriéras and were dated (Rb/Sr) at 290 ± 5 Ma (Chalier et al. 1994).

The Moulin de Chéni ore body

Structural control

The Moulin de Chéni ore body is one of several ore bodies located in the N070°E to N090°E Chéni fault zone (Fig. 3). Late N000°E to N030°E sinistral faults offset the ore bodies. The Moulin de Chéni deposit is an about 300-m-long quartz vein, trending N070°E with a 45°NW dip, with a thickness ranging from several tens of centimeters to several meters. It was mined from 1997 to 2000 yielding 2,750 kg of gold with an average grade of 12.5 g/t. The vein formed during successive compressional events (sub-horizontal shortening) and coeval quartz deposition in tension fractures (Nicaud and Floc'h 2000). The quartz vein is located at the boundary between the peraluminous Chéni granite in the footwall and micaschists of the Lower Gneiss Unit in the hanging wall. Close to the fault zone, the wall rocks contain a network (stockwork like) of cm-sized quartz-sulfide veins that are more developed in the granitic footwall than in the metamorphic hanging wall. Within a distance of about 20 m from the fault, a dense set of sulfide-dominant veins and veinlets occurs parallel to the quartz vein. The frequency of these veins decreases outward and they are absent at 30 m from the fault zone.

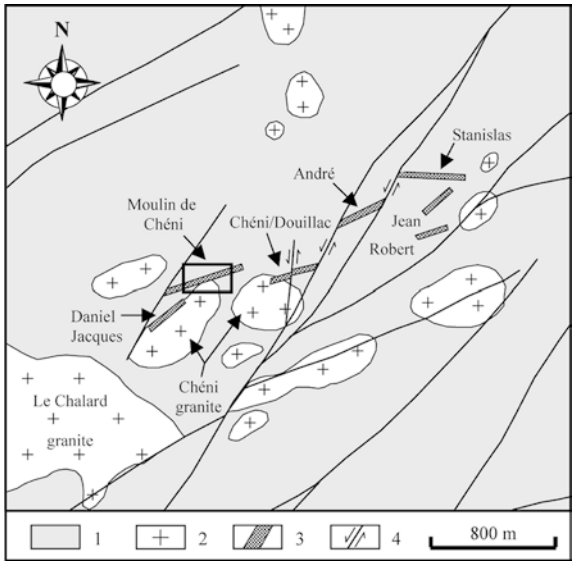

Fig. 3 Location of the main ore bodies along the Chéni fault zone with indication of the sampled area: *1* mica-rich paragneiss and micaschist, *2* peraluminous leucogranite, *3* mineralized quartz vein emphasizing the Chéni fault zone, *4* late fault with indication of the relative movement (modified from SMB-COGEMA, unpublished data)

Paragenetic sequence in the Moulin de Chéni structure

Samples were collected at two levels of the mine to interpret the paragenetic sequence in the Moulin de Chéni structure. The location of the samples is given in Fig. 4. The hydrothermal succession in the Moulin de Chéni structure may be divided into four main stages (Fig. 5):

1. Early stage: deposition of milky quartz, as both veinlets in the Chéni granite and massive filling within the fault zone. Milky quartz is the main component of the Moulin de Chéni structure and the stockwork. Under the microscope, it appears as an aggregate of anhedral to subheuhedral crystals up to 2 mm in size. Ondulatory extinction shows that the milky quartz experienced a weak ductile deformation.
2. Fe-As-S stage: brecciation of the early milky quartz is followed by coeval deposition of microcrystalline quartz (100 to 20 μm) and disseminated arsenopyrite and minor pyrite (Fig. 6A). In detail, microcrystalline

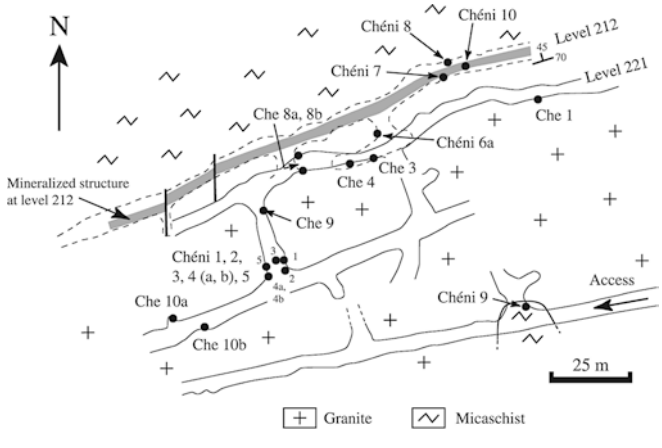

Fig. 4 Gallery map of the Moulin de Chéni underground mine with sample location. *Level numbers* refer to elevation above sea level (modified from SMB-COGEMA, unpublished data)

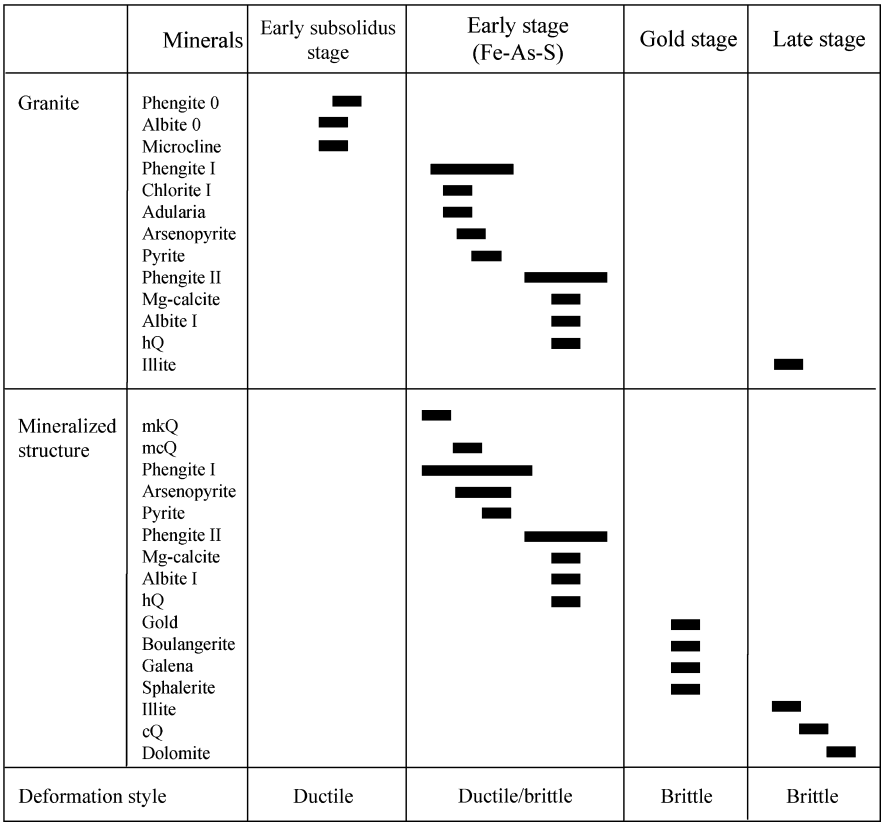

Fig. 5 Summary of the paragenetic sequence established for the mineralized structure and the granite. Host rock deformational style is indicated for each main stage. *mkQ* milky quartz, *mcQ* microcrystalline quartz, *hQ* hyaline quartz, *cQ* comb quartz

quartz and sulfides show mutual crosscutting relationships indicating repeated fracturation events. K-micas are also present and postdate sulfides. Arsenopyrite and pyrite are usually present as euhedral to subeuhedral crystals (0.5–1 mm). Arsenopyrite is the most abundant mineral and forms earlier than pyrite. Locally, arsenopyrite has grown on pyrite blades, which are probably pseudomorphs of an earlier mineral, most likely of pyrrhotite (Fig. 6B). Arsenopyrite is often twinned (hour-glass twin) and usually distinctly zoned (Fig. 6C), from zones with $As/As+S = 0.47 \pm 0.01$ to zones with $As/As+S = 0.44$ to 0.45. Its content of Sb, Ni, and Co is usually below the detection limit of the electron microprobe (1,300 ppm for Sb, 300 ppm for Co and Ni), but, locally, Sb (up to 0.3 wt%) or Co (up to 0.17 wt%) or Ni (up to 700 ppm) were found to be present. Gold is always below the detection level of 260 ppm (CAMECA SX50 microprobe, 100 nA, 25 kV, 3 min counting time). The Moulin de Chéni arsenopyrites differ from the Sb-rich and gold-bearing zoned arsenopyrites that are known from the Le Châtelet and Villeranges deposits located 70 km to the north-east (Boiron et al. 1989).

At the end of the Fe-As-S stage, the quartz vein was crosscut by mm-wide cracks sealed by hyaline quartz ± calcite ± albite, which are crosscut by illite (Fig. 6D).

3. Base metal and gold stage: base metal sulfides (sphalerite, galena) and rare sulfosalts (boulangerite) seal veinlets and dissolution patches that crosscut earlier minerals without quartz deposition. Galena clearly post-dates sphalerite, but boulangerite relationships could not be observed. Galena is enriched in both silver (up to 6,000 ppm) and bismuth (up to 1.2 wt%). Gold is present as native gold filling in microcracks of early pyrite or arsenopyrite of the Fe-As-S stage (Fig. 6 E). The chronological relationships of gold and base metal sulfides could not be observed in the Moulin de Chéni structure but they have been demonstrated to be coeval in other gold occurrences from the Saint-Yrieix district (Essarraj 1992; Essarraj et al. 2001), so we assume that gold and base metals were also contemporaneous at Moulin de Chéni.
4. Late fault infill: Comb quartz, sometimes with coeval dolomite, fills vugs, several cm-large, as a consequence of the re-opening of the main structure during extensional tectonics (Nicaud and Floc'h 2000; Nicaud 2001).

Alteration in the Chéni granite

Alteration paragenesis

An early stage of pervasive alteration is marked in the granite by: (i) growth of muscovite flakes, mostly at the expense of the magmatic biotite; (ii) replacement of K-feldspar and plagioclase by microcline (Fig. 5). All these minerals were involved in a deformation event affecting the granite at the brittle-ductile transition: undulose

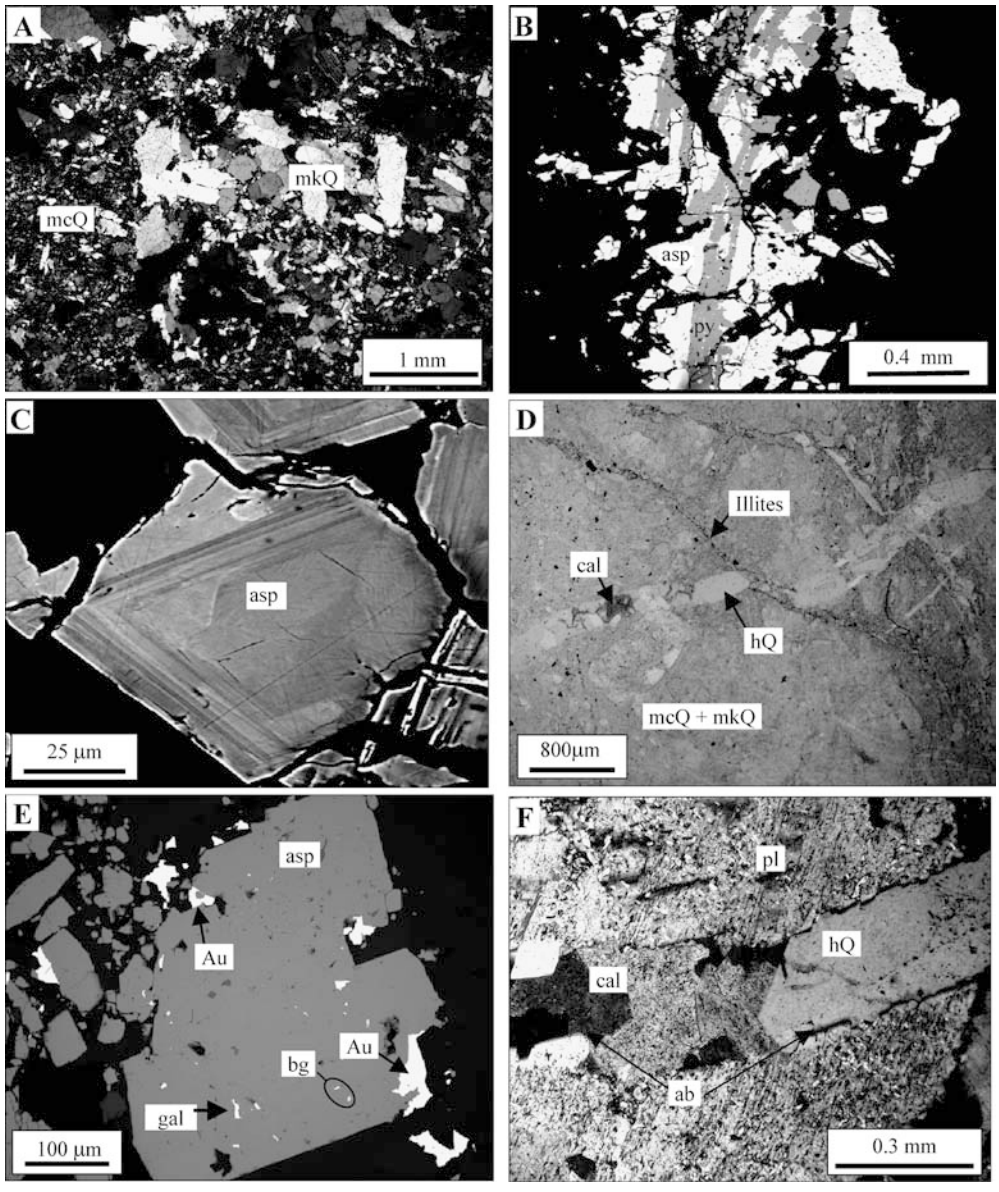

Fig. 6 Textural relationships in the mineralized quartz vein of the Moulin de Chéni deposit. **A** Early ore stage: Milky quartz cemented by microcrystalline quartz (*mcQ*). Optical microscopy; **B** Early ore stage: Arsenopyrite (*asp*) growing on pyrite (*py*) blades, the pyrite probably replacing earlier pyrrhotite. Scanning electron microscopy; **C** Arsenopyrite (*asp*) crystal showing growth zones in relation with variations of the As content. Scanning electron microscopy; **D** Early ore stage: Hyaline quartz (*hQ*) and Mg-calcite (*cal*) vein crosscutting grey quartz (mcQ + mkQ) breccia. Optical microscopy; **E** Gold stage: Native gold (*Au*) filling pores of an arsenopyrite (*asp*) crystal containing boulangerite (*bg*) and galena (*gal*) inclusions. Scanning electron microscopy; **F** Hyaline quartz (*hQ*) and Mg-calcite (*cal*) vein with re-crystallization of plagioclase (*pl*) as albite (*ab*) on the wall. Optical microscopy, *crossed polars*

extinction of the magmatic quartz, kinking of biotite and early muscovites, broken feldspars. Locally, mylonite corridors (up to a few cm thick) are observed. They are similar to the flat-lying ductile shear-zones described in the nearby Chalard granite (Lespinasse 1991). The microcrystalline quartz is demonstrably younger than these shear-zones (Nicaud 2001). Thus, the early K-alteration event preceded the onset of fracture-controlled hydrothermal circulation in the Chéni granite.

The main alteration stage is responsible for the zonal macroscopic pattern (Fig. 7A and 8) with an inner ''bleached'' zone and an outer ''greenish'' zone:

– In the inner zone, the ''bleaching'' is due to biotite replacement by K-feldspar (adularia), with residual Ti oxides (Fig. 7B). Early microcline is often recrystallized into adularia, and further replacement of plagioclase by adularia as vuggy dissolution patches may locally be seen.
– In the outer zone, the ''greenish'' alteration is due to the replacement of biotite by chlorite and Ti-oxides. Careful examination at the diffuse boundary between inner and outer zones demonstrates that chloritization in the outer zone was coeval with the ''bleaching'' process in the inner zone. Chlorite is distinctly enriched in iron (Mg number #: 0.27 to 0.30) compared to pristine biotite (Mg number #: 0.44 to 0.49).

The boundary between the ''bleached'' zone and ''greenish'' zone is rather sharp, whereas the boundary between the ''greenish'' zone and unaltered granite is diffuse. The inner ''bleached'' zone is usually about 1 cm thick. As the vein density increases toward the stockwork, alteration haloes merge and the entire granite host is ''bleached''.

These alterations post-date milky quartz and are coeval with microcrystalline quartz, arsenopyrite and

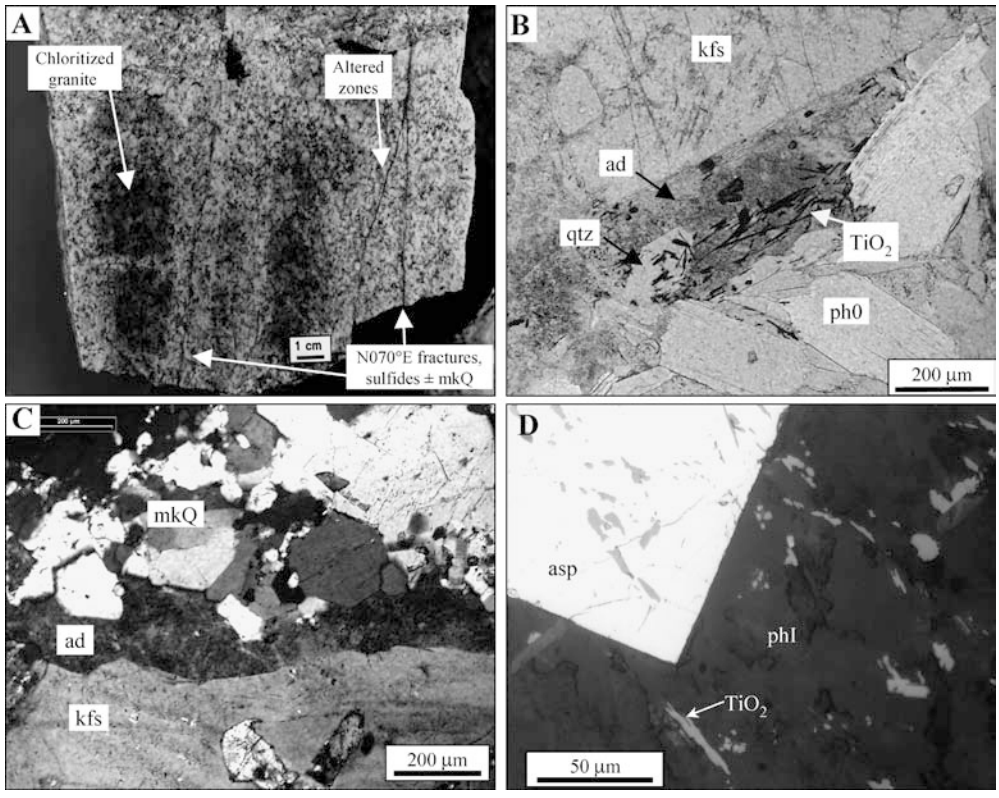

Fig. 7 Textural relationships in the altered granite: **A** N070°E sulfide vein network with alteration halos. Hand specimen; **B** Mineral assemblage in the altered zone. Biotite is replaced by adularia (*ad*). Titanium is not mobilized and crystallizes as titanium oxides (TiO_2). Phengite (*ph0*) is related to the early sub-solidus alteration stage. Optical microscopy; **C** Epitaxic development of adularia (*ad*) onto magmatic K-feldspar (*kfs*) close to the wall of the milky quartz (*mkQ*) vein. Optical microscopy, crossed polars; **D** Euhedral arsenopyrite (*asp*) crystal and coeval phengite I (*phI*). Phengite I is the result of biotite alteration as emphasized by the presence of titanium oxides (TiO_2) in the cleavage planes of phengite. Scanning electron microscope

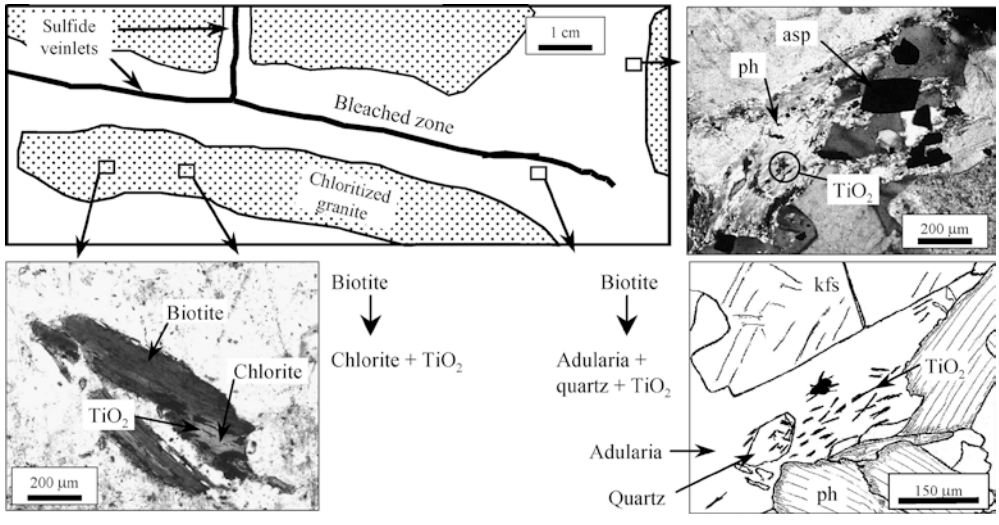

Fig. 8 Schematic representation of element migration in the altered zone. *asp* arsenopyrite; *kfs* K-feldspar; *ph* phengite; TiO_2 titanium oxides

pyrite of the Fe-As-S stage, according to the following observations: i) They clearly overprint all the early deformed minerals; ii) Brecciated milky quartz is locally dissolved/cemented by adularia (Fig. 7C); iii) When present in the Chéni granite, microcrystalline quartz-sulfide microcracks contain frequently small adularia crystals mixed with microcrystalline quartz. In the prolongation of some of these microcracks, porphyroblastic pyrite is seen to have grown in K-feldspar-replaced biotite, preserving Ti-oxide trails reminiscent of the former cleavages, and incorporating small arsenopyrite prisms spatially associated with the Ti-oxides (Fig. 7D). This indicates that growth of arsenopyrite and pyrite was coeval with the biotite dissolution.

A phengitic alteration is developed at the expense of plagioclase, but its time relationships with the alteration of biotite are difficult to establish. However, as the phengite-producing reaction involves K^+, it may be related to the biotite disappearance and/or the related K-alteration. The celadonite and paragonite content of phengite is moderate (0.28 to 0.34 and 0.01 to 0.04,

Table 1 Bulk composition of fresh and altered granite from the Moulin de Chéni gold deposit. Major elements were determined by ICP-AES and are given in oxide weight percent. Trace elements were determined by ICP-MS and are given in ppm. CO_2 and S were determined by infrared absorptiometry and are given in weight percent. *DL* detection limit. *Che10a* and *Che10b* unaltered granite; *Chéni 4b*g ranite (chloritized biotite) located 2 to 5 cm from sulfide veins with bleached walls;*Chéni 2* granite with chloritized biotite; *Chéni 4a* strongly bleached granite (1 to 3 cm thick bleached halos on the wall of sulfide veinlets) with replacement of biotite by phengite and/or adularia; *Chéni 5* bleached granite from the stockwork zone with replacement of biotite by phengite; *Chéni 6a* bleached granite from the stockwork zone (replacement of biotite by phengite and/or adularia, epitaxic overgrowths of adularia on magmatic K-feldspar and presence of some arsenopyrite crystals); *Chéni 3* Bleached granite of the stockwork zone (replacement of biotite by phengite and/or adularia and presence of arsenopyrite and carbonates)

Sample	Che10a	Che10b	Chéni 4b	Chéni 2	Chéni 4a	Chéni 5	Chéni 6a	Chéni 3
Distance from the quartz structure	30 m	30 m	20 m	20 m	20 m	15 m	10 m	15 m
Alteration style	Fresh granite		Host rock alteration Chloritized biotite		Bleached granite in stockwork zone			
SiO_2	73.83	74.00	73.16	74.75	72.97	72.90	73.72	73.58
Al_2O_3	14.48	14.29	14.58	13.22	14.38	14.36	13.74	14.38
Fe_2O_3t	1.66	1.58	1.34	1.02	1.20	1.38	1.47	1.57
MnO	< DL	< DL	0.03	0.04	< DL	0.03	< DL	< DL
MgO	0.30	0.29	0.47	0.39	0.46	0.59	0.31	0.36
CaO	0.99	0.79	0.65	0.59	0.53	0.69	0.34	0.17
Na_2O	4.02	3.89	3.55	3.33	3.71	3.31	2.84	1.25
K_2O	3.70	4.04	4.47	4.19	4.66	4.79	5.17	6.36
TiO_2	0.17	0.16	0.11	0.07	0.11	0.11	0.11	0.11
P_2O_5	0.07	0.08	0.10	0.11	0.12	0.10	0.10	0.1
L.O.I	0.70	0.77	1.42	1.33	1.67	1.97	1.65	1.98
Total	99.93	99.91	99.88	99.04	99.83	100.23	99.45	99.86
CO_2 tot (%)	0.07	0.04	0.41	0.50	0.59	0.75	0.07	0.08
S tot (%)	0.03	0.05	0.22	0.24	0.35	0.45	0.50	0.49
Ba	1327	1276	763	483	706	788	784	880
Be	5.4	4.8	4.7	5.7	3.5	3.6	3.4	4.1
Bi	0.1	1.1	1.6	2.5	1.2	1.6	1.9	2.0
Co	1	1	1	1	1	1	1	1
Cr	13	8	14	11	< DL	15	11	14
Cu	< DL	< DL	5.0	6.0	< DL	< DL	7	< DL
Ga	17.6	18.0	20.2	21.3	17.8	19.6	19.0	20.3
Mo	0.7	1.1	0.7	0.5	0.4	1.5	1.4	1.5
Nb	8.4	10.6	13.2	15.1	12.3	12.8	13.2	13.5
Ni	5	< DL	6	< DL	< DL	6	< DL	6
Pb	82	80	78	68	67	79	63	70
Rb	170.7	182.1	181.9	205.0	191.3	187.4	204.4	264.3
Sb	1.2	2.0	6.1	10.8	15.5	11.7	23.0	30.2
Sn	3.3	3.3	6.6	10.1	5.9	5.7	5.9	54.1
Sr	370	342	186	110	153	162	158	128
V	5	5	5	4	7	5	8	12
Y	5.2	5.6	16.9	14.1	16.0	15.3	19.2	14.7
Zn	56	45	39	101	31	23	13	61
Zr	119	110	69	59	65	84	104	82
U	13.9	14.1	14.3	14.0	12.3	16.4	17.9	17.0
Th	36.0	34.2	13.1	8.6	11.2	14.5	15.1	14.9
W	3.3	4.0	5.9	6.1	7.3	7.9	6.7	12.1
As	77.4	115.7	1294	2722	3679	2325	4457	6022
La	38.9	35.5	26.4	17.8	24.0	28.9	30.6	30.3
Ce	65.8	60.7	49.9	34.3	44.9	55.3	57.9	57.5
Pr	6.28	5.80	5.12	3.38	4.76	5.62	6.03	5.80
Nd	20.5	19.2	18.5	12.3	17.6	19.2	20.0	20.7
Sm	2.85	2.80	3.64	2.53	3.16	3.69	4.07	3.73
Eu	0.81	0.78	0.79	0.53	0.71	0.76	0.78	0.95
Gd	1.95	1.75	3.09	2.21	2.66	2.92	3.38	2.80
Tb	0.26	0.25	0.53	0.38	0.44	0.48	0.55	0.46
Dy	1.17	1.14	2.80	2.17	2.71	2.51	3.29	2.43
Ho	0.17	0.17	0.59	0.47	0.48	0.54	0.61	0.49
Er	0.41	0.46	1.43	1.14	1.34	1.42	1.64	1.30
Tm	0.06	0.06	0.25	0.19	0.20	0.23	0.27	0.21
Yb	0.45	0.45	1.35	1.18	1.34	1.37	1.65	1.18
Lu	0.07	0.08	0.21	0.18	0.19	0.19	0.26	0.19
Density (g/cm^3)	2.63	2.63	2.65	2.65	2.65	2.64	2.66	2.67

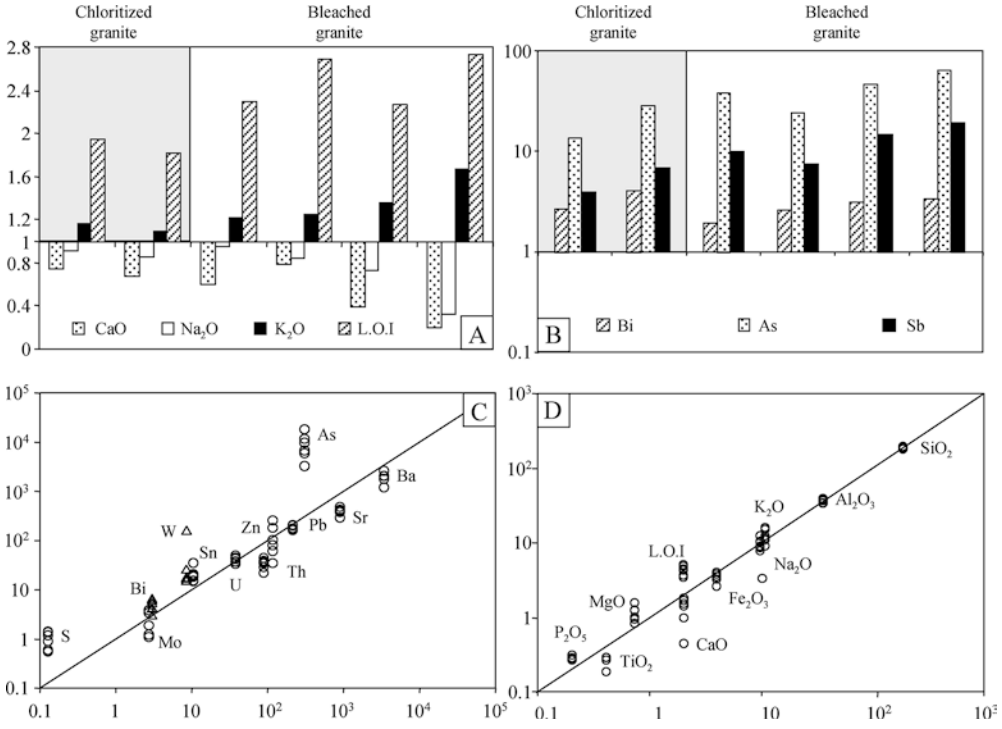

Fig. 9 Gains and losses of major and minor elements. Concentration of elements has been corrected for density. **A** and **B**: chemical profile from chloritized granite to bleached granite in the stockwork zone (concentrations are normalized to the fresh parental granite). **C** and **D**: isocon diagrams (element concentration in altered sample versus element concentration in fresh granite) for all analyzed samples. Line 1:1 is the iso-chemical line, and elements plotting under and above that line are lost or gained, respectively (Grant 1986). *L.O.I.* loss on ignition

respectively) and the magnesium content is relatively high when compared to biotite and chlorite.

Late hydrothermal circulation in the Chéni granite may be coeval with similar events in the Moulin de Chéni structure. Quartz ± albite ± calcite veinlets (Fig. 6F) correspond to hyaline quartz in the Moulin de Chéni structure and late illite veinlets occur both in the granite and the Moulin de Chéni structure.

Geochemistry

Mass transfer during the alteration processes has been documented through chemical analyses of a set of representative samples from both the fresh granite, taken 25–30 m away from the Moulin de Chéni structure, the altered granite (''bleached'' and chloritized zones) containing quartz-sulfide veinlets and the altered granite in the well developed stockwork zone, 10 to 15 m away from the Moulin de Chéni structure. Brief sample descriptions and chemical analyses are presented in Table 1.

Specific gravities range from 2.63 to 2.67, indicating nearly isovolumetric transfer during rock alteration. The fresh granite yields the lower value (2.63) and the most altered samples, the highest ones (2.65 to 2.67). This can be explained by the introduction of early sulfides (arsenopyrite, pyrite) and by the destruction of phyllosilicates (biotite, chlorite) in favor of adularia during alteration. The little variation in specific gravities is consistent with the rock textures being preserved in spite of progressive mineral replacement.

Chemical gains and losses are presented graphically in Fig. 9. Na and Ca are strongly depleted and K is enriched, in good correlation with an increase of the L.O.I. These changes are related to the breakdown of plagioclase and the introduction of K. The other major elements, Si, Al and Ti remain practically constant. Mg-enrichment is likely related to crystallization of Mg-rich phengite. The near constancy of iron despite the biotite destruction is evidence for the sequestration of the released iron by coeval crystallization of arsenopyrite and pyrite, with concomitant enrichment in S and As.

Some trace elements such as Ba and Sr are depleted, which is probably related to the breakdown of plagioclase. HREE are enriched while LREE remain constant (Table 1). Metals, such as Bi, Sb (present within sulfides), Sn and W are enriched. Zn and Pb, present as sulfides in the vein system, display an erratic behavior.

Two conclusions seem particularly relevant for the understanding of the hydrothermal system at Moulin de Chéni: (i) As, S, Bi and Sb were added to the rock during the alteration process; (ii) iron released by biotite breakdown was sulfidized to form pyrite, and arsenic was incorporated into arsenopyrite.

Characterization of fluid inclusions

Petrography and microthermometry of fluid inclusions have been carried out on thick oriented wafers (200 μm) from representative samples of the host granites, micaschists, and quartz veins.

Fluid inclusions were studied by microthermometry using a Chaixmeca stage (Poty et al. 1976) for the freezing and a Fluid Inc. stage for the heating experiments. Salinity in weight percent equivalent NaCl (wt%

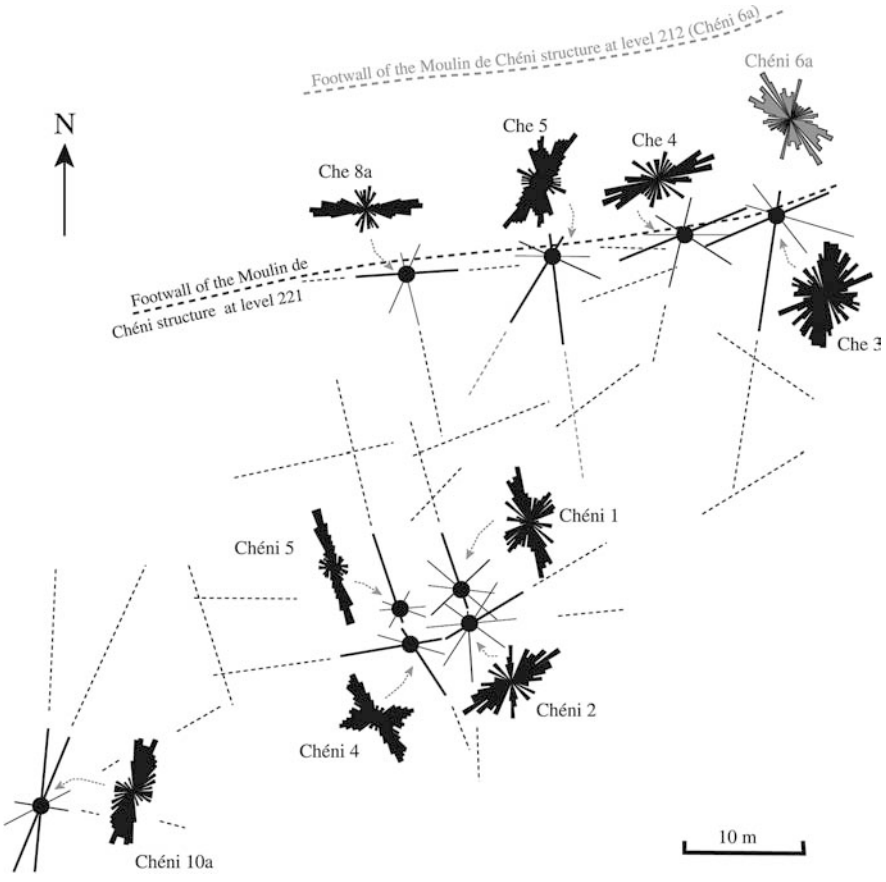

Fig. 10 Rose diagrams representing the orientation of the fluid inclusion planes in the magmatic quartz of the granite. *Dashed lines* schematically indicate the preferential fluid pathways

eq. NaCl) was calculated by the equation of Bodnar (1993). In volatile-bearing fluid inclusions, CO_2 was detected by melting of the solid phase below –56.6°C. The volumetric fraction of the volatile phase has been estimated at room temperature by reference to the volumetric chart of Roedder (1984). The analyses of the gas phase were performed using a Dilor Labram Raman spectrometer following the procedure given by Dubessy (1984). Bulk compositions were determined using thermodynamic codes from Thiéry et al. (1994) and Bakker (1997). Isochores were calculated using the program of Bakker (1999) or the data from Zhang and Frantz (1987).

Typology

Most fluid inclusions found in this study were formed during the healing of fluid inclusion planes (FIP) in the host quartz.

Volatile-bearing inclusions are observed both in quartz from a metamorphic enclave (sample Chéni 9) and in the magmatic quartz from the granite, particularly in the ''bleached'' granite, as 10 to 15 μm-large fluid inclusions showing negative crystal to irregular shapes. They are also found in the milky quartz and in the hyaline quartz, but their small size (< 4 μm) precluded their study. All the fluid inclusions are two- or three-phase at room temperature (liquid H_2O, vapor $CO_2 \pm$ liquid CO_2). When they are three-phase fluid inclusions with a volatile/water ratio ranging from 0.3 to 1 they are named Lc-w, and Vc-w when the vapor/liquid ratio exceeds 0.5 and homogenization is to the vapor state. They are named Lc when H_2O is absent (two-phase inclusions) and homogenization is to the liquid state.

Aqueous inclusions are two-phase with vapor/liquid ratios ranging from 0.1 to 0.3. They homogenize to the liquid state and are named Lw. Some of them are present as primary inclusions in the late comb quartz, and are named Lw2, in order to be singled out from the other aqueous inclusions (Lw1) occurring as FIP in other types of quartz and in wall-rocks.

Geometry and time relationships of fluid migration

Lespinasse and Pecher (1986) showed that the direction of the FIP might be related to the stress field because they correspond to tension gashes. Thus, P-T-X conditions for each stage of fluid percolation in the host granite may be attributed to a tectonic event assuming that FIP directions represent paleostress fields. Identification and geometric characterization of the FIP were carried out on oriented horizontal wafers using an interactive videographic analyzer (Nogueira and Noronha 1995).

All measured FIP are vertical to subvertical, allowing presentation of the direction measurements in statistical rose diagrams (Fig. 10). Two main sets of directions (N060°–N080°E and N160°–N010°E) are ubiquitous, but at a given locality, the FIP pattern displays many minor directions. Such a complexity reflects both changes of the main stress direction in time and local stress re-orientation at the vicinity of pre-existing fractures especially in the stockwork zone.

The two sets of directions can be correlated to two structural deformation events at the mine scale (Nicaud 2001). The N060–080°E direction is the shortening direction related to the dextral activity of the Moulin de Chéni structure, whereas the N160°–N010°E direction corresponds to the reworking of the Moulin de Chéni structure by late normal-sinistral brittle faults (Fig. 3).

The volatile-bearing FIP are restricted to the early N060°–080°E directions. They are particularly abundant in the magmatic quartz of the K-altered granite close to the N070°E sulfide ± quartz veins. They are also present in microcrystalline quartz and milky quartz. Therefore, these fluids are interpreted as responsible for the K-alteration and As-Fe-S hydrothermal stage.

The Lw1 FIP are present in all orientations but are most characteristic of the N160°–010°E set. They clearly overprinted the volatile-bearing PIF, meaning that the N060°–080°E direction was re-opened at the time of the aqueous fluid circulation. As a consequence, the aqueous fluids percolated through a network of roughly orthogonal microcracks, whereas the circulation of the previous fluids was restricted to a set of microfractures, more or less parallel to the main structures (Fig. 10). The circulation of Lw1 fluids is earlier than the late comb quartz deposition and FIP are commonly found paralleling sulfide-healed microcracks in milky quartz. This indicates that Lw1 fluids spanned the late base metal and gold stage.

Microthermometry and Raman microspectrometry

Microthermometric and Raman data are summarized in Tables 2 and 3.

Lc-w fluid inclusions from metamorphic quartz exhibit melting temperatures of CO_2 (Tm CO_2) between −59.3 and −56.8 °C. Homogenization temperatures of CO_2 (Th CO_2) to the liquid or the vapor phase range from 8.6 to 31 °C. Melting temperatures of clathrate (Tm cl) range from 6.4 to 11.2 °C. Decrepitation occurs prior to homogenization in the range of 300–350 °C for most of the inclusions. One homogenization temperature (Th) to the aqueous liquid phase was observed at 372 °C.

Lc-w, Vc-w and Lc fluid inclusions in the K-altered granite show Tm CO_2 ranging from −60.9 to −57.2°C and Th CO_2 to the liquid or the vapor phase in the range of 10.4 to 26.5 °C. Tm cl ranges from 2.8 to 10.8 °C. Th ranges from 360 to 410 °C either to the liquid or to the

Table 2 Summary of fluid inclusion types and coeval mineral assemblages from the Moulin de Chéni deposit with microthermometric data and fluid inclusion plane (FIP) orientations. For each microthermometric parameter, ranges and mode (in parenthesis) are given.*TmCO*$_2$ melting temperature of solid CO_2. *Th* CO_2 homogenization temperature of CO_2. *Tm ice* melting temperature of ice. *Tm cl* melting temperature of clathrate. *Th* homogenization temperature. Homogenization mode: *L* liquid. *C* critical. *V* vapor. All values are in °C. Nomenclature for fluid inclusions is explained in the text

Stage	Fluid inclusions					Microthermometric data			FIP orientations
	Habitus	Type	Tm CO_2	Th CO_2	Tm cl	Tm ice	Th	
Late metamorphic stage and early ore stage								
Gneiss	Secondary	Lc-w, Vc-w	−56.8/−59.3	8.6/31 L or V	6.4/11.2 *(5/6 and 8/9)*		290/362 (L)	Unoriented sample
Granite	Secondary	Lc-w, Vc-w, Lc	−57.2 / -60.9	10.4 / 26.5 L or V *(25 ± 2)*	2.8/10.8 *(4/5 and 8/9)*		330/410 L or V	N060–080°E
Base metal and gold stage	Secondary inhost rocks and milky quartz	Lw1				−0.9 / −5.2	140/290 (L or V)	N160–010°E ± N060–080°E
Late barren stage	Primary in comb quartz, secondary in host rocks and milky quartz	Lw2				−0.5 / 0.9	150/210 (L)	N160–010°E ± N060–080°E

Table 3 Chemical compositions obtained by Raman microprobe spectroscopy of selected fluid inclusions and corresponding microthermometric data from the Moulin de Chéni deposit. Compositions are given in mole%.*TmCO*$_2$ melting temperature of solid CO_2.*ThCO*$_2$ homogenization temperature of CO_2. *Tm ice* melting temperature of ice. *Tm cl* melting temperature of clathrate. *Th* homogenization temperature. Homogenization mode: *L* liquid.*C* critical. *V* vapor. Decrepitation temperatures are indicated with an asterisk. All values are in °C. *n.o.* not observed

Quartz type	Sample	Inclusion	Fluid type	Microthermometry						Raman data (volatile phase)			Bulk composition				
				Tm CO_2	Th CO_2	Mode	Tm cl	Th	Mode	CO_2	CH_4	N_2	H_2O	CO_2	CH_4	N_2	NaCl
FIP in metamorphi cquartz lenses	Chéni 9	a1	Lc–w	−57.3	30.5	V	8.7	320*	L	90.3	4.6	5.1	91.0	7.5	0.2	0.3	1.0
		a4b	Lc–w	−57.2	31.0	V	8.2	320*	L	89.9	2.9	7.2	87.4	10.2	0.3	0.7	1.4
		a5b	Lc–w	−57.2	31.0	C	6.6	320*	L	95.2	1.2	3.6	90.5	7.2	0.0	0.2	2.1
		a8	Lc–w	−57	23.5	C	6.5	320*	L	100.0	0.0	0.0	92.8	5.2	0.0	0.0	2.0
		a11b	Lc–w	−56.8	n.o		9.5	320*	L	91.1	8.9	0.0	94.4	4.8	0.2	0.0	0.6
		b1b	Lc–w	−58.2	23.0	L	7.0	320*	L	85.5	4.7	9.8	78.2	17.0	0.8	1.8	2.2
		b4	Lc–w	−58.1	23.5	V	7.4	372	L	85.5	6.9	7.6	92.1	5.4	0.2	0.3	2.0
		b5b	Lc–w	−57.8	24.0	L	7.2	350*	L	84.9	3.8	11.3	83.8	12.3	0.4	1.4	2.1
		a12b	Lc–w	−56.8	17.0	V	9.7	300*	L	79.2	9.2	11.6	94.4	4.3	0.2	0.3	0.8
FIP in granite	Che3	8	Lc–w	−57.7	22.0	V	7.9	270*	L	92.1	4.3	3.6	88.9	9.3	0.3	0.3	1.2
		6	Vc–w	−57.4	26.1	C	4.5	405	V	95.4	1.8	2.8	82.6	13.8	0.2	0.4	3.0
		7	Vc–w	−57.4	26.0	C	2.8	410	V	96.0	1.0	3.0	82.4	13.4	0.1	0.3	3.8
		10	Vc–w	−57.2	26.2	C	4.5	376	V	94.5	1.6	3.9	82.1	14.2	0.2	0.5	3.0
		1	Vc–w	−57.9	25.8	L	3.6	390*	V	95.0	1.5	3.5	69.0	26.8	0.4	0.9	2.9
	Che4	13	Lc–w	−57.7	22.8	C	8.8	>330	L	93.6	4.3	2.1	88.4	10.1	0.3	0.2	1.0
		1	Vc–w	−57.9	25.4	C	8.9	334*	V	93.0	2.4	4.6	68.9	28.2	0.7	1.3	0.9
		9	Vc–w	−58.1	23.7	C	8.9	>330	V	93.0	4.0	3.0	84.4	13.8	0.5	0.4	0.9
		14	Vc–w	−57.8	22.2	C	8.7	330*	V	93.6	4.3	2.1	84.3	13.9	0.5	0.3	1.0
		7	Lc	−57.7	25.3	L	n.o	n.o	n.o	95.0	1.3	3.7	0.0	95.0	1.3	3.7	–
	Chéni 4	a1	Vc–w	−60.9	10.4	V	8.9	300*	V	74.2	17.7	8.1	84.7	9.5	1.8	0.4	3.6
	Chéni 2	c2	Lc–w	−59.8	16.0	V	6.6	372	L	81.9	13.8	4.3	90.0	6.6	0.7	0.2	2.5
		b0	Lc–w	−59.6	17.6	L	7.2	373	C	85.4	10.9	3.7	74.1	20.4	2.3	0.8	2.4
		a1	Vc–w	−60.5	16.3	V	7.0	300*	V	78.6	11.0	10.4	83.7	11.2	1.2	1.1	2.8
		a2	Vc–w	−60.5	17.5	V	7.2	300*	V	89.3	7.6	3.1	82.1	14.3	1.0	0.4	2.2
		b1	Vc–w	−57.7	19.3	V	7.5	365	V	88.2	7.9	3.9	74.2	21.0	1.7	0.8	2.3

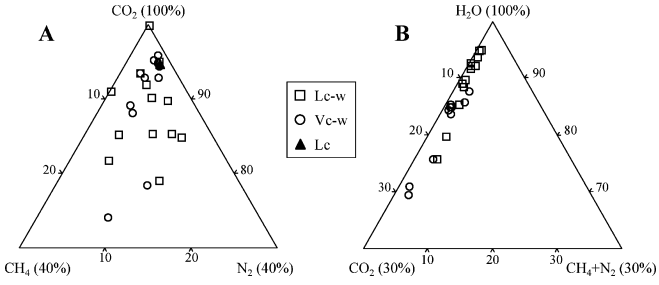

Fig. 11 Ternary plot for aqueous-carbonic fluid composition. **A** Volatile phase **B** Bulk composition

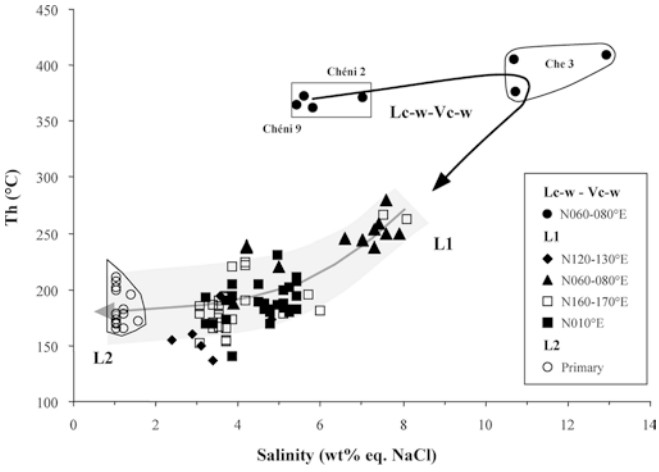

Fig. 12 Salinity-Th plot for aqueous-carbonic (Lc-w—Vc-w) and aqueous (L1 and L2) fluids. The direction of the fluid inclusion planes is indicated by the symbol style

vapor phase. Many fluid inclusions decrepitated before homogenization in the 300–390 °C range. Lc fluid inclusions have $TmCO_2$ ranging from −57.8 to −57.7 °C, and Th CO_2 to the liquid phase ranging from 23.5 to 25.7 °C. Raman analysis shows CO_2 (74.2–100 mol%) with less CH_4 (0–17.7 mol%) and N_2 (0–11.6 mol%) (Fig. 11). The bulk composition of the Lc-w and Vc-w fluid inclusions is dominated by H_2O (70–95 mol%). Salinity varies from 0.2 to 3.8 mol% NaCl.

Aqueous fluid inclusions (Lw1) show melting temperatures of ice (Tm ice) ranging from −5.2 to −0.9 °C (8.1–1.6 wt% eq. NaCl). The Th ranges between 140 and 290 °C. Lw2 inclusions show Tm ice in the range of −0.9 to −0.5 °C (1.6–0.9 wt% eq. NaCl). Th ranges from 150 to 210 °C.

The salinity versus Th diagram (Fig. 12) shows a mixing trend between a fluid having a salinity of about 8 wt% eq. NaCl (L1), close to the salinity of the earlier aqueous-carbonic fluids, and Th around 250 °C, and a dilute (ca. 1 wt% eq. NaCl) fluid (L2).

P–T-t reconstruction

The P–T reconstruction is based on the calculation of isochores for each family of fluid inclusions (Fig. 13).

Early dense volatile-rich fluids were found in the metamorphic quartz lenses. Most inclusions decrepitated before total homogenization, at a temperature of around 330 °C but a single measurement at 372 °C sets the minimum trapping temperature, at a pressure of about 240 MPa (Fig. 13A). The true trapping temperature cannot be better constrained, as no alteration assemblage is associated in time with these fluids. Aqueous carbonic fluids from the hydrothermal system were trapped in the altered granite and to a lesser extent in some metamorphic lenses. The small Th range (365–410 °C) contrasts with the spread of the minimum trapping pressures from 210 to 50 MPa (Fig. 13A). The trapping conditions are further constrained by biotite instability (chloritization), meaning that the temperature could not have exceeded 425 ± 25 °C according to the maximal thermal stability of chlorite at such pressures (Frey et al. 1991). So, the data record a near isothermal pressure drop. The flat lying isochores for either Lc-w or Vc-w FIP with homogeneous sets of fluid inclusions allow the pressure to be constrained at 75 MPa or less (Fig. 13 B). The Lc isochore is consistent with this estimate.

Some N060°–080°E FIP coeval inclusions with similar compositions exhibit highly contrasted densities (Lc-w and Vc-w inclusions b0 and b1 of the sample Chéni 2, Table 3). These inclusions suggest a re-equilibration process during uplift, with the high-density inclusions interpreted as preserved original inclusions, and the low-density inclusions being re-equilibrated. Using the equation of Bodnar et al. (1989), an inclusion like b1 (6 μm in diameter) must have experienced an internal overpressure of at least 190 MPa, corresponding with re-equilibration conditions around 75 MPa and 420 °C, which is consistent with the previous estimates.

Aqueous fluids responsible for gold deposition have minimal trapping temperatures ranging from 140 to 290 °C. The pressure could not have been in excess of the lowest pressure recorded for the preceding stage (75 MPa) and is likely to have decreased. Indeed, a pressure of 55 ± 10 MPa has been estimated for the same stage in the nearby Lauriéras deposit and for similar fluids at the regional scale (Essarraj et al. 2001; Souhassou 2001). Consequently, the trapping temperatures were likely in the 350–170 °C range (Fig. 13A). Cooling may be related to the dilution process.

Aqueous fluids observed in late comb quartz (Lw2 inclusions) have a minimum trapping temperature ranging from 150 to 210 °C. Comb quartz grew in open spaces, implying hydrostatic pressure conditions, at a structural level which remains unknown.

At a late stage of the circulation of the aqueous-carbonic fluids, the estimated pressure was as low as 75 MPa. This low pressure is unlikely to record lithostatic conditions, as there is no evidence of shallow level intrusions able to yield the 420 °C temperature at the corresponding depth of 2.8 km and this pressure must be interpreted as infralithostatic. Conversely, the high

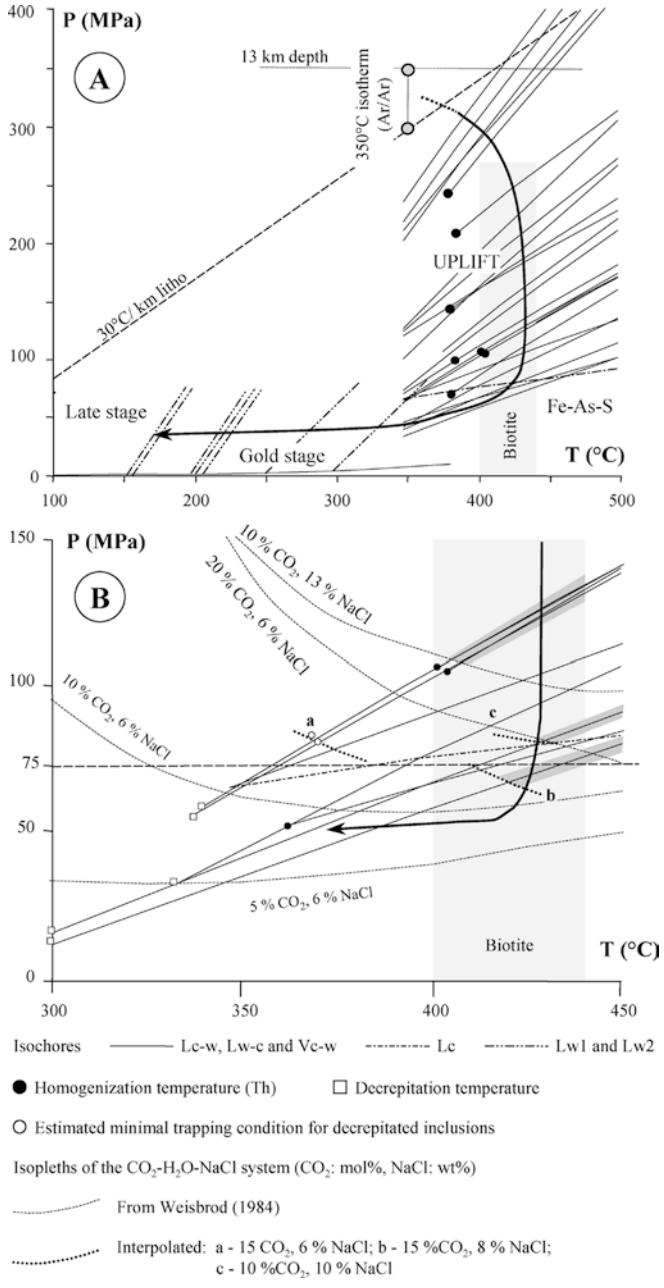

Fig. 13 P–T tracks (*arrows*) from high P–high T to low P–low T during ore deposition at Moulin de Chéni. **A** General path beginning near the pressure of peak metamorphism (13 km depth). The 350 °C isotherm corresponds to Ar/Ar closure system in white mica prior to the formation of the quartz lodes. A 30 °C/km geotherm is assumed and corresponds to a depth of 11 km. Aqueous-carbonic fluid inclusions record a slight temperature increase and a pressure drop to 70 MPa (5–6 km depth under infralithostatic regime). The fracturation of the quartz vein allows the circulation and the mixing of aqueous fluids at decreasing temperature leading to gold deposition. **B** Details of the aqueous-carbonic fluid behavior during the Fe-As-S stage. Plotted isopleths show that the variations observed in the fluid composition (see Fig. 11 and 12) may lead to local unmixing. Interpolated isopleth b gives the best constraint on the P–T conditions (around 70 MPa and 420 °C) at the end of the uplift stage

pressures recorded by the early aqueous carbonic fluids are necessarily lithostatic. During the lithostatic to infralithostatic transition, and considering the fluid compositions, the (L + V) isopleths should have been transected. Heterogeneous trapping of aqueous and carbonic fluids is poorly recorded but a few inclusions are likely to result from limited unmixing. As seen in Fig. 13B (Lc isochore), such inclusions are consistent with the estimated conditions at the end of the decompression event.

In the northwestern French Massif Central, the thickness of the lithotectonic pile was at least 13 km (Floc'h 1983), corresponding to a minimal lithostatic pressure of around 350 MPa. Furthermore, all $^{39}Ar/^{40}Ar$ ages on white micas from the metamorphic rocks, granites and pegmatites that host the auriferous quartz lodes of the Saint-Yrieix area are older than 330 Ma (Monié et al. 2000; Alexandrov 2000). This shows that the 350 °C isotherm was transected at the regional scale prior to the formation of the quartz structures and, assuming a 30 °C/km geotherm should set the initial conditions at around 300 MPa and 350 °C (Fig. 13B). Therefore, the Moulin de Chéni structure experienced an uplift of at least 4 km (from about 300 MPa to about 200 MPa) up to 7.5 km depth as a response to late Variscan extensional tectonics (Bouchot et al. 2000).

According to our findings, the fluid temperature must have exceeded 420 °C towards the end of the decompression and an assumed uplift of 4 km was likely accompanied by a thermal input at depth. In the northwest of the Massif Central abnormal heat flow was advocated at the end of the Carboniferous on the basis of numerical modeling and thermochronological data by Scaillet et al. (1996). An uplift of 0.3 mm/year could have maintained the high temperature in the deep upper crust. Alternatively, heat advection by the fluids could be related to broad thermal gradients around granitic intrusions, as proposed in the northwestern French Massif Central in order to explain the so-called "episyenite" alteration, due to percolation of fluids ≥350 °C at pressures ≤ 50 MPa (Lespinasse 1991; André et al. 1999).

Origin of fluids: oxygen isotope geochemistry of quartz

$^{18}O/^{16}O$ ratios were measured on bulk quartz samples, as well as on separated quartz chips extracted from fluid inclusion wafers. The analytical procedure follows the conventional fluorination method of Clayton and Mayeda (1963) and is given in Bernard-Griffiths et al. (1996).

A summary of the $\delta^{18}O$ vs. SMOW data of quartz and estimated crystallization temperature deduced from the fluid study are given in Table 4. Using the quartz-H_2O fractionation curve of Zheng (1993), the calculated $\delta^{18}O$ values of the corresponding hydrothermal fluids were estimated, with the following results:

Table 4 Summary of oxygen isotope data for the different quartz generations of the Moulin de Chéni deposit. $\delta^{18}O$ values for fluids are calculated using estimated crystallization temperature of quartz from fluid inclusion studies and the quartz-H_2O fractionation curve from Zheng (1993). *mkQ* milky quartz; *mcQ* microcrystalline quartz; *hQ* hyaline quartz; *cQ* comb quartz. The standard is SMOW

Quartz type	Sample reference	Comment	$\delta^{18}O$ Qtz	Estimated crystallization temperature	$\delta^{18}O$ fluid
Metamorphic quartz	Chéni 9	Wafer	12.09	375 ± 25 °C	6.5–7.6
mkQ	Chéni 6a	Bulk	16.10	425 ± 25 °C	11.6–12.4
mkQ	Chéni 6a	Wafer	16.15	425 ± 25 °C	11.6–12.5
mkQ	Chéni 3	Wafer	15.50	425 ± 25 °C	11–11.8
mkQ	Chéni 7	Wafer	15.24	425 ± 25 °C	10.7–11.6
mcQ	Chéni 10	Bulk	12.24	420 ± 5 °C	8–8.2
mcQ	Chéni 8b	Bulk	12.78	420 ± 5 °C	8.5–8.7
mcQ	Chéni 2	Wafer	12.88	420 ± 5 °C	8.6–8.8
hQ	Chéni 10	Bulk	13.15	380 ± 20 °C	7.8–8.6
cQ	Che1	Wafer	11.90	220 ± 20 °C	0.3–2.5
cQ	Chéni 7	Wafer	12.38	220 ± 20 °C	0.7–3

1. The metamorphic quartz was deposited from a CO_2-bearing fluid with $\delta^{18}O$ of the water component between 6.5 and 7.6‰; these values fix the composition of the metamorphic fluids in the Moulin de Chéni area.
2. The milky quartz crystallized from a CO_2-bearing fluid with $\delta^{18}O$ of the water component ranging from 10.7 to 12.5‰ corresponding to a fluid equilibrated with basement lithologies such as granitoids (Kerrich 1987).
3. The late comb quartz was deposited from a fluid with $\delta^{18}O$ between 0.3 and 3‰, which may be interpreted as a surface-derived fluid (''meteoric water'') that experienced weak interaction with basement lithologies. This fluid corresponds to the L2 end-member involved in the cooling and mixing process related to the gold deposition (Fig. 12).
4. The microcrystalline and hyaline quartz were deposited from fluids with $\delta^{18}O$ values ranging from 8.5 to 8.8‰ and from 7.8 to 8.6‰, respectively. These values are significantly lighter than that for the milky quartz stage and could be the result of CO_2 unmixing. However, we do not find an indication of a generalized unmixing process in the studied fluid inclusions.

The ''hot and saline'' L1 end-member fluid was not accompanied by quartz deposition and it is not possible to get a direct estimate of its $\delta^{18}O$ value. Nevertheless, the data of the present study are similar to that obtained in the nearby Lauriéras gold deposit by Essarraj et al. (2001) for a similar hydrothermal circulation history. At Lauriéras, it was possible to get an estimate for the mixed fluids of the base metal and gold mineralizing stage, with $\delta^{18}O$ values ranging from 9 to 4‰. Essarraj et al. (2001) interpret these results as a mixing between a ''hot and saline'' end-member with $\delta^{18}O$ close to 9‰ or a fluid equilibrated with basement lithologies and a ''cold and low-saline'' end-ember with $\delta^{18}O$ close to 4‰ or a ''meteoric-exchanged'' fluid. Given the overall similarities between the Lauriéras and Moulin de Chéni deposits, we think that the same interpretation holds at Moulin de Chéni.

Discussion and conclusion

The following scenario of fluid circulation was reconstructed for the Moulin de Chéni deposit:

1. Early fluid circulation is focussed in a N070°-090°E regional (initially ductile) fault structure and coeval and parallel sets of tension microcracks, in a basically transpressive regime (Nicaud and Floc'h 2000; Nicaud 2001). The fluids were CO_2-rich and equilibrated at depth with the regional lithotypes (''pseudometamorphic'' fluids). They mainly deposited quartz, in decreasing abundance with time and formed the mineralized lodes. They were also responsible for the bleaching of the granite along the quartz structure. The early fluid circulation accounts for the partial to complete destruction of biotite and plagioclase, the neoformation of K-feldspar and phengite, and precipitation of arsenopyrite and pyrite.
2. Late circulation of aqueous fluids is more pervasive and controlled by a dense interconnected set of microcracks; with reopening of earlier microcracks, together with the creation of a dominant set of N160°–N010°E FIP paralleling coeval normal-sinistral brittle faults. The trapped fluids record a mixing process, between a ''saline'' end-member (L1, ≥8 wt% eq. NaCl) and a low-salinity end-member (L2, ≤ 0.5 wt% eq. NaCl), the latter being of surface origin (''meteoric''), while the former is likely to be akin to ''pseudometamorphic'' fluids.

These mixed fluids mainly deposited sphalerite, galena, boulangerite, and gold. Gold deposition on fractures in sulfides of the Fe-As-S stage is probably controlled by electrochemical properties (Möller and Kersten 1994).

The reconstructed P–T-t path for the fluids in the Moulin de Chéni structure shows a significant pressure drop (from about 300 MPa down to 75 MPa). This points to rapid uplift, consistent with the inception of extensional tectonics at local (Nicaud and Floc'h 2000; Nicaud 2001) and regional (Bouchot et al. 1989) scale. The decompression occurred at rather constant

temperatures (between 370 and 420 °C) implying sustained high heat flow. This suggests abnormally heated rocks at depth, either because of the rapid uplift, or due to the presence of concealed magmatic intrusions.

These successive circulation events are not an isolated process restricted to the Moulin de Chéni deposit but are typical of the whole Saint-Yrieix district (Boiron et al. 2000; Fourcade et al. 2000; Essarraj et al. 2001; Vallance 2001), including the surrounding area (Souhassou 2001). The granite-hosted Moulin de Chéni deposit is not an intrusion-related gold deposit in the sense of Lang and Baker (2001). The same fluid evolution was encountered at the scale of the West European Variscan Belt, from northwestern Iberia (Boiron et al. 1996) to Bohemia (Boiron et al. 2001; Vallance 2001; Boiron et al. 2003) implying the existence of crustal-scale hydrothermal systems operating at the end of the Variscan orogenesis.

According to the model of a crustal-scale continuum of hydrothermal systems from the lower crust up to the surface evoked for Archean cratons (Groves 1993; Cassidy et al. 1998, Groves et al. 1998), gold may be deposited in a wide range of crustal environments and over a temperature and pressure range from 250 to 600 °C and 100 to 400 MPa via sulphidation reactions. On the other hand the Variscan orogenic gold deposits are characterized by two major contrasted stages with gold deposition during a late stage of fluid mixing in a shallow crustal environment. According to the classification of Groves et al. (1998), the two stages of evolution of the Variscan gold deposits consist of an early ''mesozonal'' stage of quartz-sulfide (Fe-As-S) deposition, usually devoid of gold (formation of the structural and chemical trap) followed by a late ''epizonal'' stage of base metal and gold deposition. This leads to the definition of a ''Variscan type of shear zone-hosted gold deposits'' (Bonnemaison et Marcoux 1989; Cathelineau et al. 1991; Marignac et al. 2000; Essaraj et al. 2001).

Acknowledgements Funding for this research was provided by grants from the GeoFrance 3D program and the regional project ''Massif Central 3D Mapping and Metallogeny'' and the French Research group on Ore deposits ''TRANSMET'' (GDR CNRS-n°2458). The company ''Société des Mines du Bourneix'' is thanked for having permitted sampling in the mine. Juliette Nicaud is especially acknowledged for her technical and scientific assistance during field work. The authors are grateful to Susanne Schmidt for improving the manuscript. This paper has significantly benefited from the constructive reviews of Odin Christensen, Bernd Lehmann and Eric Marcoux.

References

Alexandrov P (2000) Géochronologie U/Pb et 40Ar/39Ar de deux segments de la chaîne Varisque: le Haut Limousin et les Pyrénées orientales. PhD Thesis, Nancy University, France

André AS, Lespinasse M, Cathelineau M, Boiron MC, Cuney M, Leroy J (1999) Percolations de fluides tardi-hercyniens dans le granite de Saint Sylvestre (Nord-Ouest du Massif Central Français): données des inclusions fluides sur un profil. C R Acad Sci Paris 329:23–30

Arthaud F, Matte P (1977) Late Palaeozoic strike-slip faulting in Southern Europe and Northern Africa: result of a right-lateral shear zone between the Appalachian and the Urals. Geol Soc Am Bull 88:1305–1312

Bakker RJ (1997) Clathrates: computer programs to calculate fluid inclusions V-X properties using clathrate melting temperature. Comp Geosci 23:1–18

Bakker RJ (1999) Adaptation of the Bowers and Helgeson (1983) equation of state to the H_2O-CO_2-CH_4-N_2-NaCl system. Chem Geol 154:225–236

Bernard-Griffiths J, Fourcade S, Peucat JJ, Kienast JR, Martineau F, Rahmani A (1996) Geochemistry and isotope (Sr, Nd, O) study of Al-Mg ganulites from the In Ouzzal Archean Block (Hoggar, Algeria). J Metamorphic Geol 14:709–724

Bodnar RJ (1993) Revised equation and table for determining the freezing point depression of H_2O-NaCl solutions. Geochim Cosmochim Acta 57:683–684

Bodnar RJ, Binns PR, Hall DL (1989) Synthetic fluid inclusions VI. Quantitative evaluation on the decrepitation behaviour of fluid inclusions in quartz at one atmosphere, confining pressure. J Metamorphic Geol 7:229–242

Boiron MC, Barakat A, Cathelineau M, Banks DA, Durisova J, Moravek P (2001) Geometry and P-V-T-X conditions of microfissural ore fluid migration: the Mokrsko gold deposit (Bohemia). Chem Geol 173:207–225

Boiron MC, Cathelineau M, Banks DA, Fourcade S, Vallance J (2003) Mixing of metamorphic and surficial fluids during the uplift of the Hercynian upper crust: consequences for gold deposition. Chem Geol 194:119–141

Boiron MC, Cathelineau M, Banks DA, Vallance J, Fourcade S, Marignac C (2000) Behaviour of fluids in Variscan crust during late Carboniferous: uplifting and fluid mixing and their consequences on metal transfer and deposition. In: Bouchot V, Moritz R (eds) A GEODE-GEOFRANCE 3D workshop on orogenic gold deposit in Europe with emphasis on the Variscides., Orléans, pp 56–57

Boiron MC, Cathelineau M, Banks DA, Yardley BWD, Noronha F, Miller MF (1996) P-T-X conditions of late hercynian fluid penetration and the origin of granite hosted gold quartz veins in northwestern Iberia : a multidisciplinary study of fluid inclusions and their chemistry. Geochim Cosmochim Acta 60: 43–57

Boiron MC, Cathelineau M, Trescases JJ (1989) Conditions of gold-bearing arsenopyrite in the Villeranges basin, Marche-Combrailles shear zone, France : a mineralogical and fluid inclusions study. Econ Geol 84:1340–1362

Boiron MC, Essarraj S, Sellier E, Cathelineau M, Lespinasse M, Poty B (1992) Identification of fluid inclusions in relation with their host microstructural domains in quartz by cathodoluminescence. Geochim Cosmochim Acta 56:175–185

Bonnemaison M, Marcoux E (1989) Auriferous mineralization in some shear-zones: a three-stage model of metallogenesis. Miner Deposita 25:96–104

Bouchot V, Gros Y, Bonnemaison M (1989) Structural controls on the auriferous shear zones of the Saint-Yrieix District, Massif Central, France: evidence from the Le Bourneix and Lauriéras gold deposits. Econ Geol 84:1315–1327

Bouchot V, Milési JP**,** Ledru P, Lerouge C, Roig JY, Bellot JP, Becq-Giraudon JF, Truffert C (2000) Orogenic gold veins and W, Li-F mineralizations related to ''specialised'' granites: two markers of the crustal scale Au-W-Sb metalliferous peak at 310–305 Ma (French Variscan Belt). In: Bouchot V, Moritz R (eds) A GEODE-GEOFRANCE 3D workshop on orogenic gold deposit in Europe with emphasis on the Variscides., Orléans, pp 53–55

Cassidy KF, Groves DI, McNaughton NJ (1998) Late-Archean granitoid-hosted lode-gold deposits, Yilgarn Craton, Western Australia: deposit characteristics, crustal architecture and implications for ore genesis. Ore Geol Rev 13:65–102

Cathelineau M, Marignac C, Boiron MC, Poty B (1991) Hercynian gold bearing quartz veins from Western Europe: the ''shear zone model'' revisited. Proceeding of Gold 91, Brazil, Balkema, pp 115–119

Chalier M (1993) Contexte géologique, géochimique et structural des lentilles aurifères de Lauriéras et Puit-Roux (Limousin Central, District de Saint-Yrieix). Implications métallogéniques. PhD Thesis, Limoges University, France

Chalier M, Virlogeux D, Duthou JL (1994) Les lamprophyres du district aurifère de Saint-Yrieix (Limousin, Massif Central Français). Age Rb/Sr Autunien et relation chronologiques avec le dépôt de l'or. C R Acad Sci Paris 319:1511–1518

Clayton RN, Mayeda TK (1963) The use of bromine and pentafluorine in the extraction of oxygen from oxides and silicates for isotopes analysis. Geochim Cosmochim Acta 27:43–52

Dubessy J (1984) Simulation des équilibres chimiques dans le système C-O-H. Conséquences méthodologiques pour les inclusions fluides. Bull Mineral 107:155–168

Essarraj S (1992) Migration des fluides, microfissuration et conditions de dépôt de l'or dans les veines de quartz aurifères. PhD Thesis, Nancy University, France

Essarraj S, Boiron MC, Cathelineau M, Fourcade S (2001) Multistage deformation of Au-quartz veins (Lauriéras, French Massif Central): evidence for late gold introduction from microstructural, isotopic and fluid inclusion studies. Tectonophysics 336:79–99

Floc'h JP (1983) Le socle métamorphique du Limousin central: une traverse de la zone ligérienne de l'orogenèse varisque de l'Aquitaine à la zone broyée d'Argentat (Massif Central français). Thesis, Limoges University, France

Fourcade S, Boiron MC, Cathelineau M, Guerrot C, Lerouge C, Marignac C, Martineau F, Vallance J (2000) Fluids and late Carboniferous Variscan gold mineralizations in the French Massif Central. The bearing of stable isotopes. In Bouchot V Moritz R (eds) A GEODE-GEOFRANCE 3D workshop on orogenic gold deposit in Europe with emphasis on the Variscides., Orléans, pp 58–59

Frey M, de Capitani C, Liou, JG (1991) A new petrogenetic grid for low-grade metabasites. J Metamorphic Geol 9:497–509

Grant JA (1986) The isocon diagram, a simple solution to Gresens's equation for metasomatic alteration. Econ Geol 81:1976–1982

Groves DI (1993) The crustal continuum model for late-Archaean lode-gold deposits of the Yilgarn Block, Western Australia. Miner Deposita 28:366–374

Groves DI, Goldfarb RJ, Gebre-Mariam M, Hagemann SG, Robert F (1998) Orogenic gold deposits: a proposed classification in the context of their crustal distribution and relationship to other gold deposit types. Ore Geol Rev 13:7–27

Kerrich R (1987) Stable isotope study of fluids in the crust. In: Kyser TK (ed) Short course on stable isotope geochemistry in low temperature fluids. Miner Assoc Can Saskatoon, pp 258–286

Lafon JM, Respaut JP (1988) Géochronologie U-Pb et leucogranites Varisques: cas des massifs de Grandrieu (Lozère) et de La Porcherie (Limousin), Massif Central Français. Bull Min 111:225–237

Lang JR, Baker T (2001) Intrusion-related gold systems: the present level of understanding. Miner Deposita 36:477–489

Ledru P, Autran A, Santallier D (1994b) Lithostratigraphy of Variscan terranes in the French Massif Central: a basis for paleogeographical reconstruction. In: Keppie JD (ed) Pre-Mesozoic geology in France and related areas. Springer, Berlin Heidelberg New York, pp 276–288

Ledru P, Costa S, Echtler H (1994a) The massif central: structure. In: Keppie JD (ed) Pre-Mesozoic geology in France and related areas. Springer, Berlin Heidelberg New York, pp 305–323

Lespinasse M (1991) Les traînées d'inclusions fluides: marqueur microstructural des paléocontraintes et migrations fluides. Mem Géologie et Géochimie des Matières Premières et Energétiques 19

Lespinasse M, Pecher A (1986) Microfracturing and regional stress field: a study of preferred orientations of fluid inclusion planes in a granite from the Massif Central, France. J Struct Geol 8 (2):169–180

Marignac C, Cathelineau M, Boiron M C, Fourcade S, Vallance J, Souhassou M (2000) The Q-Au lodes of W Europe: towards the definition of a variscan type of shear zone hosted gold deposit. In Bouchot V, Moritz R (eds) A GEODE-GEOFRANCE 3D workshop on orogenic gold deposit in Europe with emphasis on the Variscides. Orléans, pp 82–85

Marignac C, Cuney M (1999) Ore deposit of the French Massif Central: insight into the metallogenesis of the variscan collision belt. Miner Deposita 34:472–504

Matte P (1991) Accretionary history and crustal evolution of the Variscan belt in western Europe. Tectonophysics 196: 309–337

Möller P, Kersten G (1994) Electrochemical accumulation of visible gold on pyrite and arsenopyrite surfaces. Miner Deposita 29:404–413

Monié P, Respaut JP, Brichaud S, Bouchot V, Faure M, Roig JY (2000) 40Ar/39Ar and U-Pb geochronology applied to Au-W-Sbmetallogenesis in the Cévennes and Châtaigneraie districts (Southern Massif Central, France). In: Bouchot V, Moritz R (eds) A GEODE-GEOFRANCE 3D workshop on orogenic gold deposit in Europe with emphasis on the Variscides., Orléans, pp 77–79

Nicaud J (2001) Analyse de la fracturation des filons aurifères de Moulin de Chéni, Puits-Roux et Fagassière. Contrôle structural des minéralisations aurifères (Limousin, Haute-Vienne). PhD Thesis, Limoges Universty, France

Nicaud J, Floc'h JP (2000) Structural control of gold-bearing quartz veins forming in the Saint-Yrieix District (Massif Central, France). In: Bouchot V, Moritz R (eds) A GEODE-GEOFRANCE 3D workshop on orogenic gold deposit in Europe with emphasis on the Variscides. Orléans, pp 71–72

Nogueira P, Noronha F (1995) "Planif" a computer program for the study of fluid inclusion planes. Bol Soc Esp Min 18:182–186

Pastier P (1992) Typologie des granitoides de l'Ouest du Massif Central Français. Géochimie et minéralogie des granites alumineux. Evolution épigénétique dans le district de Saint-Yrieix. PHD Thesis, Limoges University, France

Poty B, Leroy J, Jachimowicz L (1976) Un nouvel appareil pour la mesure des températures sous le microscope: l'installation de microthermométrie Chaixmeca. Bull Soc Fr Min Cristallogr 99:182–186

Roedder E (1984) Fluid inclusions. Rev Mineral 12: Miner Soc Am

Santallier D, Briand B, Ménot RP, Piboule M (1988) Les complexes leptyno-amphiboliques (C.L.A): revue critique et suggestions pour un meilleur emploi de ce terme. Bull Soc Géol Fr 8 (IV): 3–12

Scaillet S, Cuney M, Le Carlier de, Veslud C, Cheilletz A, Royer JJ (1996) Cooling pattern and mineralization history of the Saint-Sylvestre and Western Marche leucogranite pluton, French Massif Central. II. Thermal modelling and implications for the mechanisms of uranium mineralization. Geochim Cosmochim Acta 60:3887–3907

Souhassou M (2001) Les circulations fluides dans le bâti Sud-Limousin à la fin du Carbonifère: relations entre les systèmes hydrothermaux de la faille d'Argentat et Saint-Yrieix; conséquences pour la métallogénie de l'or. PhD Thesis, Nancy University, France

Stussi JM, La Roche H (1984) Le magmatisme granitique orogénique de la chaîne varisque française. Typologie chimique et répartition spatiale. C R Acad Sci Paris 298:43–48

Thiéry R, Vidal J, Dubessy J (1994) Phase equilibria modelling applied to fluid inclusions: liquid-vapour equilibria and calculation of the molar volume in the CO_2-CH_4-N_2 system. Geochim Cosmochim Acta 58:1073–1082

Touray JC, Marcoux E, Hubert P, Proust D (1989) Hydrothermal processes and ore-forming fluids in the Le Bourneix gold deposit, Central France. Econ Geol 84:1328–1339

Vallance J (2001) Les paléofluides de la fin de la collision varisque: evolution pression-température-composition et rôle métallogénique. Une étude pluridisciplinaire des districts à Au d'Europe occidentale. PhD Thesis, Nancy University, France

Weisbrod A (1984) Utilisation des inclusions fluides en géothermobarométrie. In: Lagache M (ed) Thermométrie et barométrie géologiques Soc Fr Min Cristallogr 2:415–459

Zhang YG, Frantz JD (1987) Determination of the homogenization temperatures and densities of supercritical fluids in the system NaCl-KCl-$CaCl_2$-H2O using synthetic fluid inclusions. Chem Geol 64:335–350

Zheng YF (1993) Calculation of oxygen isotope fractionation in anhydrous silicate minerals. Geochim Cosmochim Acta 56:1079–1091